



HAL
open science

Faster Simulation Approach Dedicated to Infrared Thermographic Inspection of Anisotropic Delaminated Planar Pieces

Valentin Noël

► **To cite this version:**

Valentin Noël. Faster Simulation Approach Dedicated to Infrared Thermographic Inspection of Anisotropic Delaminated Planar Pieces. 2024. hal-04372603

HAL Id: hal-04372603

<https://hal.science/hal-04372603v1>

Preprint submitted on 4 Jan 2024

HAL is a multi-disciplinary open access archive for the deposit and dissemination of scientific research documents, whether they are published or not. The documents may come from teaching and research institutions in France or abroad, or from public or private research centers.

L'archive ouverte pluridisciplinaire **HAL**, est destinée au dépôt et à la diffusion de documents scientifiques de niveau recherche, publiés ou non, émanant des établissements d'enseignement et de recherche français ou étrangers, des laboratoires publics ou privés.

Faster Simulation Approach Dedicated to Infrared Thermographic Inspection of Anisotropic Delaminated Planar Pieces

Valentin Noël

SATIE

Ecole Normale Supérieure Paris-Saclay

Laboratoire des Signaux et Systèmes

Université Paris-Saclay, CentraleSupélec

Gif-sur-Yvette, France

valentin.noell@ens-paris-saclay.fr

Abstract—In this work, we propose an analytical model based on an approximation of the heat transfer within a part by successive and simultaneous convolution operations for the simulation of thermographic inspection (single or double-sided). Infrared thermography has already proven to be an important method for non-destructive evaluation, due to the fact that it provides information in an immediate, fast and low cost manner. The temperature distribution is approximated by its expansion on a tensor. The configurations treated by this model are laminated flat parts affected by thin delamination defects. The sources considered are lamps providing thermal excitation to the surface of the inspected part. The description of the delamination defects as thin air gaps between the layers of the part is equivalent to the introduction of a surface resistance to the thermal flow, thus allowing their treatment by the modal approach applied without additional discretization. The proposed model, although developed particularly for fibrous polymeric materials, has been generalized to be applicable to all types of materials (i.e. (an-)isotropic).

Index Terms—non-destructive testing, infrared thermography, anisotropic materials, isotropic materials

I. INTRODUCTION

Thermal/infrared non-destructive testing (T/INDT) techniques have received increasing attention in recent years due to their advantages of fast, high-resolution, non-contact testing and technical advances in infrared cameras and data acquisition equipment. The detection of irregularities is based on the principle that all bodies emit infrared radiation when their temperature is above 0 K. The emitted infrared radiation can be measured by infrared cameras, and the images are then analyzed for defect detection and characterization. Irregularities present within the part under study affect the rate of heat diffusion, resulting in thermal contrast on the surface(s) of the part. By analyzing the alterations or contrast in the thermal pattern of the material surface, information about subsurface defects can be obtained. The simulation of TNDT procedures involves, in a first step, the solution of the thermal conduction problem in the considered part, with and without defects, in order to obtain the temperature distribution at the interfaces of the part, which constitutes the measurement. The

complete solution of this problem can be obtained by using a numerical technique such as the finite element method (FEM) or the finite integration technique (FIT) [1]. Nevertheless, in practical situations, it is often useful to forgo the detailed information of the full numerical solution in favor of fast analytical or semi-analytical approximations, like the TREE approach proposed in [2], which retain the essence of the heat flow behavior. In other words, the popularity of FEM and FIT methods is only matched by their robustness and large computational cost. This paper proposes an analytical model based on an approximation of the heat transfer equation by successive convolution operations. This singular approach, stemming from an intuition and from the approach used by Comsol for the modelling of convective exchanges as put forward in [3], is based on a homogenization of the constitutive parameters of the fibered polymeric materials (CFRP) with the final objective of being a reliable method while remaining from a computational point of view very light, which would help to tend towards a fast use and thus perfectly adapted to the generation of data sets for inverse problems.

II. CONDUCTION HEAT TRANSFER IN (IN-)HOMOGENEOUS MATERIALS

To calculate the temperature field in homogeneous materials, the classical heat conduction solutions have been summarized by Carslaw and Jaeger [4]

$$\frac{1}{a^{(i)}} \frac{\partial T^{(i)}(x, y, z, t)}{\partial t} = \frac{\partial^2 T^{(i)}(x, y, z, t)}{\partial x^2} + \frac{\partial^2 T^{(i)}(x, y, z, t)}{\partial y^2} + \frac{\partial^2 T^{(i)}(x, y, z, t)}{\partial z^2}, \quad i = 1, \dots, M \quad (1)$$

$$T^{(i)}|_{t_0} = T_{in} \quad (2)$$

$$T^{(i)}|_{z_j} = T^{(i+1)}|_{z_j} \quad (3)$$

$$-\sigma^{(i)} \frac{\partial T^{(i)}}{\partial z} \Big|_{z_j} = -\sigma^{(i+1)} \frac{\partial T^{(i+1)}}{\partial z} \Big|_{z_j} \quad (4)$$

- $T^{(i)}$ temperature in the i -region
- M number of layers
- T_{in} initial piece temperature
- $a^{(i)} = \sigma^{(i)} / (\rho^{(i)} C_p^{(i)})$ thermal diffusivity in the i -region

These equations are therefore applicable in the case where the material of interest is homogeneous. In the case where we are interested in anisotropic materials, these equations are no longer applicable. Indeed, in the case of isotropic materials, the observed thermal conductivity is a scalar (varying or invariant depending on the assumptions). In other words, whatever the direction from which we observe the heat flow, the conductivity will be identical in the whole material, independently of the direction and the layer studied. On the other hand, in the case of polymeric materials reinforced by fibers (carbon, glass, etc.), the conductivity σ is no longer representable as a scalar [5] and [6]. Indeed, in a CFRP material, each layer is composed of an alignment of carbon fibers located within a matrix (considered here as epoxy), each layer having its own fiber orientation. The thermal conductivity within the epoxy matrix is of the order of $\sigma_m = 0.25 W/mK$, within the carbon fiber $\sigma_f = 129 W/mK$.

Therefore, the use of a scalar conductivity is impossible. Let us observe a square cell of surface S , composed of an epoxy matrix representing a surface S_1 and a carbon fiber of surface S_2 . The fraction of surface of the fiber is thus equal to $S_f = \frac{S_2}{S_1 + S_2}$. If we consider a square piece of length L , $V_f = S_f * L$. Therefore, to determine the thermal conductivity $\sigma_{//}$ parallel to the fiber

$$\sigma_{//} = \sigma_f V_f + (1 - V_f) \sigma_m \quad (5)$$

Following the same logic, we can determine the transverse conductivity k_{\perp}

$$\frac{1}{\sigma_{\perp}} = \frac{V_f}{\sigma_f} + \frac{(1 - V_f)}{\sigma_m} \quad (6)$$

It is important to note that this value is the lower limit of the transverse conductivity. This homogenization allows us to define the parameters $\sigma_{//}$ and σ_{\perp} as a function of the conductivities of the epoxy matrix σ_m and of the fiber σ_f , with the knowledge a priori of a ratio of 5 between the parallel and transverse conductivities. One of the major points of contention in the estimation of thermal conductivities is the necessity to consider a conductivity through fold σ_{CP} such that $\sigma_{CP} \neq \sigma_{CP}$ or not. In this paper, we consider a conductivity $\sigma_{CP} \neq \sigma_{CP}$. From these newly defined parameters, it is now possible to define the different conductivities in any direction of the part as a function of the orientation θ of the carbon fibers of the studied layer, as first introduced in [7]

$$\bar{\sigma} = \begin{pmatrix} \sigma_{//} \cos^2 \theta + \sigma_{\perp} \sin^2 \theta & \frac{\sigma_{//} - \sigma_{\perp}}{2} \sin 2\theta & 0 \\ \frac{\sigma_{//} - \sigma_{\perp}}{2} \sin 2\theta & \sigma_{//} \cos^2 \theta + \sigma_{\perp} \sin^2 \theta & 0 \\ 0 & 0 & \sigma_{CP} \end{pmatrix} \quad (7)$$

with $\bar{\sigma}$ the conductivity tensor, which will be used for the Comsol implementation when declaring the conductivities in the layer.

This approach, called homogenization, leads to several remarks. Such an approach allows us to simplify the architecture of our part by allowing us to no longer consider the epoxy matrix and the carbon fiber separately. This has the effect of facilitating the implementation of finite element approaches such as Comsol and simultaneously decreasing the required computational costs. However, the disadvantage of homogenization is that it brings some additional uncertainty to the model of the part, which was estimated at about 4% dans [8].

III. CONVOLUTION APPROACH

The development of convolution kernels for this application consists of three steps. The heat transfer in a CFRP material composed of several plies is defined as follows: for each ply, different influences are to be considered: the heat transfer from the layer above and the layer below, as well as the heat transfer in the layer itself. In the case of the presence of defect(s) at the interfaces surrounding the studied layer, the influence of these defects must also be taken into account.

Therefore, we can divide the different influences into five distinct parts:

- influence layer $n - 1$
- influence layer $n + 1$
- influence layer n
- influence of defects on interfaces n and $n + 1$

These influences are characterized by the layer from which the incoming heat transfer originates. That is, the influence of the $n - 1$ layer is characterized by the $n - 1$ layer and thus the convolution kernel corresponding to this layer. Similar reasoning is applied for the $n + 1$ layer. As for the other influences, they are all characterized by the studied layer, the n layer. Thus, in the case where we study the n layer such that the $n - 1$ and $n + 1$ layers exist, five influences and three convolution kernels will be used. In the case where the $n - 1$ or $n + 1$ layer does not exist (edges of the part), only four influences take place and two convolution kernels are used.

These convolution kernels are developed as follows: each layer has the same conductivity components in the direction of the fiber and orthogonal to it. However, each layer has its own fiber orientation. With this information, it is possible to define the convolution kernels corresponding to each of these layers. Indeed, with the expression of the Gaussian kernel being:

$$G_{2D}(x, y; \sigma_{sd}) = \frac{1}{2\pi\sigma_{sd}^2} e^{-\frac{x^2 + y^2}{2\sigma_{sd}^2}} \quad (8)$$

with σ_{sd} the standard deviation, σ_{sd}^2 the variance, we can determine the Gaussian kernel for zero orientation with the parallel and transverse conductivities $\sigma_{/}$ and σ_{\perp} :

$$G_{2D}(x, y; \sigma_{sd}) = \frac{1}{2\pi\sigma_{sd}^2} e^{-\frac{\sigma_{\perp} \times x^2 + \sigma_{//} \times y^2}{2\sigma_{sd}^2}} \quad (9)$$

To obtain the convolution kernels oriented according to the fiber orientation, it is sufficient to define the fiber orientation for each layer and to perform a rotation of the same angle to the convolution kernel.

In order to visualize the implementation more easily, pseudo-code algorithms are available in Alg.1, 2 and 3. The kernels have been named as follows in our implementation:

- h_1 : convolution kernel of the layer $n - 1$
- h_2 : convolution kernel of the layer n
- h_3 : convolution kernel of the layer $n + 1$

It is necessary to note that these kernels are normalized and that the sum of the three kernels (thus the three influences) is unitary

$$\sum_{i=1}^3 \sum_{l=1}^L \sum_{w=1}^W h_i(l, w) = 1 \quad (10)$$

where L is the length and W is the width of the top surface of the part under study.

Algorithm 1 Pseudo-code for heat transfer model for $n \neq (1, 10)$

```

1: procedure HEAT TRANSFER( $C, I, h_1, h_2, h_3, \tau_{obs}, \Delta\tau$ )
2:   while  $j < \frac{\tau_{obs}}{\Delta\tau}$  do
3:      $C_n^{\tau+1} \leftarrow C_n^{\tau} * h_2 + (C_n^{\tau} \times \sim I_n) * h_2 + (C_n^{\tau} \times \sim I_{n+1}) * h_2 + (C_{n-1}^{\tau} \times I_n) * h_1 + (C_{n+1}^{\tau} \times I_{n+1}) * h_3$ 
4:      $j \leftarrow j + 1$ 
5:   end while
6:   return  $C_n$ 
7: end procedure

```

Algorithm 2 Pseudo-code for heat transfer model for $n = 1$

```

procedure HEAT TRANSFER( $C, h_1, h_2, h_3, \tau_{obs}, \Delta\tau$ )
2:   while  $j < \frac{\tau_{obs}}{\Delta\tau}$  do
3:      $C_n^{\tau+1} \leftarrow C_n^{\tau} * h_2 + (C_n^{\tau} \times \sim I_n) * h_2 + (C_n^{\tau} \times \sim I_{n+1}) * h_2 + (C_{n+1}^{\tau} \times I_{n+1}) * h_3$ 
4:      $j \leftarrow j + 1$ 
5:   end while
6:   return  $C_n$ 
end procedure

```

One of the problems we have encountered is the setting of the standard deviation σ . Empirically, we observe that the value leading to the lowest estimation error is $\sigma = 2.1$, or $\sigma = k_{//} - k_{\perp}$.

A. Convolution approach: hypothesis

The presented approach, called convolution, calculates at each time step the temperature evolution within each layer of the studied part. The constraint of this approach is that the temperatures given in such a context are the temperatures at

Algorithm 3 Pseudo-code for heat transfer model for $n = 10$

```

procedure HEAT TRANSFER( $C, h_1, h_2, h_3, \tau_{obs}, \Delta\tau$ )
   while  $j < \frac{\tau_{obs}}{\Delta\tau}$  do
3:      $C_n^{\tau+1} \leftarrow C_n^{\tau} * h_1 + (C_n^{\tau} \times \sim I_n) * h_2 + (C_n^{\tau} \times \sim I_{n+1}) * h_2 + (C_{n-1}^{\tau} \times I_n) * h_1$ 
        $j \leftarrow j + 1$ 
   end while
6:   return  $C_n$ 
end procedure

```

the center of each layer. Thus, in order to perform the different convolution operations simulating the heat transfer within the studied material, it is necessary to initialize the temperature within the first layer. Similar to the implementation in Comsol, both the ambient temperature and the initial temperature of the part are equal to $T_0 = 25^{\circ}C$.

To do this, we will first determine the evolution of the temperature on the upper and lower surfaces of the top layer of our model, of thickness L_1 , using the equations in [1]. If we call the initial temperature distribution on the top surface of an isotropic material of thickness L_1 , $T(x, 0)$, the temperature distribution on this same surface at any other time t is given by Carslaw and Jaeger in [4] as:

$$T(x, t) = \frac{1}{L} \int_0^L T(x, 0) dx + \frac{2}{L} \sum_{n=1}^{\infty} \exp\left(\frac{-n^2 \pi^2 \alpha t}{L^2}\right) \times \cos\frac{n\pi x}{L} \int_0^L T(x, 0) \cos\frac{n\pi x}{L} dx, \quad (11)$$

where α is the thermal diffusivity in cm^2/s . The power density Q of the energy source is here expressed in cal/cm^2 . The assumption made here is that if Q is instantaneously and uniformly absorbed by a small thickness g at the top surface ($x = 0$) of the part under study, the temperature distribution at that instant is given by:

$$T(x, 0) = Q/\rho C g \quad \text{for } 0 < x < g$$

$$T(x, 0) = 0 \quad \text{for } g < x < L$$

With this initial condition, the equation 11 can be written as:

$$T(x, t) = \frac{Q}{\rho C L} \left[1 + 2 \sum_{n=1}^{\infty} \cos\frac{n\pi x}{L} \frac{\sin(n\pi g/L)}{(n\pi g/L)} \times \exp\left(\frac{-n^2 \pi^2}{L^2}\right) \right] \quad (12)$$

where ρ is the density in g/cm^3 and C is the specific heat in $cal/g^{\circ}C$. Because g is very small for opaque materials, the simplification $\sin(n\pi g) \simeq n\pi g$. Moreover, with thermal conductivity $K = \alpha\rho C$ and a pulse duration τ , giving a Dirac pulse energy $W = Q \times \tau$, the equation 12 can be written:

$$T(x, t) = \frac{W\alpha}{KL} \left[1 + 2 \sum_{n=1}^{\infty} \exp\left(\frac{-n^2\pi^2}{L^2}\right) \right] \quad (13)$$

The knowledge of these different parameters and that of the thermal diffusivity of the material ($a = 3.15 \times 10^{-7} \text{ m}^2/\text{s}$) allows us to determine the evolution of the temperature at the point of impact of the flash lamp beam on the upper surface of the part via the equation Eq.14 and the temperature of the lower surface via the equation Eq.15 in [9]:

$$T = \frac{Wa}{\sigma_{CP}L} \left(1 + 2 \sum_{n=1}^{\infty} e^{-n^2\pi^2 F_0} \right) \quad (14)$$

$$T = \frac{Wa}{\sigma_{CP}L} \left(1 + 2 \sum_{n=1}^{\infty} (-1)^n e^{-n^2\pi^2 F_0} \right) \quad (15)$$

with $F_0 = \frac{a\tau}{L^2}$ the Fourier number and σ_{CP} being the conductivity through plies.

From the equation 15 it is thus possible to determine the temperature evolution of the lower and upper surface of the first layer of our part. This information will allow us to define two key parameters for our convolution approach.

Indeed, the fact that we have the temperature evolution of the lower surface of the first layer of the part allows us to determine when is observable the first temperature rise on the lower surface. This first temperature rise being observed at a time $t = \Delta\tau$, we can thus consider that the necessary time step between each operation of calculation of heat transfer from layer to layer is carried out in a periodic way with a period equal to $\Delta\tau$. The knowledge of the time step allows us to define another parameter. Our convolution approach thus carries out the convolution operations in a periodic way with a period $\Delta\tau$, the initialization of the temperature of the upper layer of our part must correspond to the temperature at the center of this same layer at $t = \Delta\tau$. Thus, by taking again the equation Eq.13 and by replacing the length of a layer L by the value of the half of its length ($L/2$), we obtain the evolution of the temperature at the center of the first layer, with as particular interest the temperature at $t = \Delta\tau$, which will be the initial temperature of the first layer of our model.

IV. NUMERICAL SIMULATIONS

In this section, the different implementations and the characteristics related to the numerical simulations performed will be described. It is important to note that for all the parametric values given, these are common to both implementations: the first one with our convolution approach and the second one with Comsol Multiphysics.

A. Material characteristics

The purpose of this sub-section is to define the thermal constants (conductivities, densities, specific heats) and the geometries of the parts, their organizations and the characteristics of the defects. For the different numerical simulations, we will use three different solids: steel, aluminum and CFRP. The delaminations are considered as exclusively composed of

air. The characteristics of these different solids and gases are available in the table Tab.I for homogeneous materials and in the table Tab.II.

Isotropic Materials Characteristics			
Material	Thermal Conductivity σ [W/mK]	Density ρ	Heat Capacity C_p
Steel	44.5	7850	475
Aluminium	237	2707	897
Air	0.02454	1.1843	1005

TABLE I: Isotropic Materials Characteristics

Anisotropic Material Characteristics			
Material	Thermal Conductivity σ [W/mK]	Density ρ	Heat Capacity C_p
CFRP	$\sigma_{//} = 2.71, \sigma_{\perp} = 0.61, \sigma_{CP} = 0.53$	1530	917

TABLE II: Anisotropic Materials Characteristics

The choice was made to give all test pieces the same surface size. Depending on the materials used, the thickness of each part differs, as shown in Table Tab.III.

Studied Layers Geometries			
Material	Width [mm]	Height [mm]	Thickness [mm]
Steel	50	50	2.5
Aluminium	50	50	2.5
CFRP	50	50	0.2

TABLE III: Studied Layers Geometries

During the different numerical simulations, different configurations and positions of defects in the studied parts will be tested. We will therefore refer to the names given in the table Tab.IV for each delamination.

Studied Defect Characteristics [mm]				
Name	Width	Height	Depth	Thickness
Defect 1	10	10	0.4	10^{-3}
Defect 2	6	10	0.4	10^{-3}
Defect 3	10	10	0.2	10^{-2}
Defect 4	6	10	0.6	10^{-2}

TABLE IV: Studied Defect Characteristics

More specifically, during the CFRP study, different fiber stacking sequences will be implemented, with their complete description according to the corresponding numerical simulation in the table Tab.V.

Carbon-Fiber Reinforced Polymer Piece	
Number of layers	Stacking Sequence
4	$[0^\circ, 45^\circ, 90^\circ, -45^\circ]$

TABLE V: Carbon-Fiber Reinforced Polymer Piece, Characteristics

The number of layers for each of the studied parts has been determined in an arbitrary way, as the proposed approach can deal with a theoretically unlimited number of layers, with for example a material having 22 layers in [10].

B. Flash lamp characteristics

Several types of illumination can be considered in a thermal inspection framework. In the proposed case, we use a flash lamp, a frequently used approach, because of its simple mathematical modeling [11] and [12].

The source considered for the thermal inspection is a flash lamp located at 40 cm from the studied part. The surface illuminated by this lamp is a spatial support of slightly smaller dimension than the surface of the studied part. As described, the studied parts having been arbitrarily chosen of surface $50 \times 50 \text{ mm}$, the corresponding spatial support is here of $46 \times 46 \text{ mm}$. The illumination on this spatial support, which is assumed and described as uniform, corresponds to a pulse of duration $\Delta\tau$ with a power density Q . All the quoted parameters are grouped in the table Tab.VI.

Flash Lamp Characteristics	
Heat source center [mm]	(25,25)
Spatial Support (width \times height [mm])	(46 \times 46)
Heating Pulse density [W/m^2]	10^6
Heating time τ [s]	10^{-3}

TABLE VI: Flash lamp characteristics

C. Comsol hypothesis

In addition to the parameters shared and described by Tab.I-V, the Comsol Multiphysics implementation has other subtleties.

The numerical solution proposed by COMSOL Multiphysics is based on a finite element method (FEM). In the case of our study, we have performed a heat transfer study in solids (module "Heat Transfer in Solids"). The boundary conditions chosen are the so-called Dirichlet conditions, as expressed in [13]

$$T^{(i)}|_{x=0} = T^{(i)}|_{x=L} = 0 \quad (16)$$

$$T^{(i)}|_{y=0} = T^{(i)}|_{y=W} = 0 \quad (17)$$

where L and W are the height and width of the room respectively.

Like the Comsol Multiphysics implementation, the same boundary conditions are applied in the implementation of the convolution approach.

The equation observed by COMSOL Multiphysics is:

$$\rho C_p \frac{\partial T}{\partial t} + \nabla \cdot q = Q \quad (18)$$

$q = -\bar{\sigma} \nabla T$, $\bar{\sigma}$ tenseur des conductivités.

First, we have defined the architecture of our part. Our part is a layered material, each layer having a thickness of 0.2 mm . Each delamination is implemented as a thin layer (Thin Layer mode) of resistance $R_s = d_s/\sigma_s$, d_s its thickness and σ_s its thermal conductivity, modeled as a surface condition

$$-\mathbf{n}_d \cdot \mathbf{q}_d = -\frac{T_u - T_d}{R_s} \quad (19)$$

$$-\mathbf{n}_u \cdot \mathbf{q}_u = -\frac{T_d - T_u}{R_s} \quad (20)$$

Subsequently, we define a spatial support of ($46 \times 46 \text{ mm}$) using the plane creation tool. In the analysis, it is assumed that the spatial support is uniformly heated. This is an idealized situation. On this plane is defined a surface illumination by a flash lamp of power density $Q = 10^6 \text{ W/m}^2$ for a duration of $\tau = 1 \text{ ms}$. To do this, a step function of amplitude Q and duration τ have been implemented. The corresponding equation is:

$$-n \cdot q = Q_b \quad (21)$$

avec $Q_b = Q\delta(t - \tau)$, [W/m^2].

In order to compare the heat transfer results of Comsol vs. our method, the study was given the same time step as the one used by our method.

D. Comsol: comparisons

This sub-section is reserved for the comparison of the temperature evolution results at the bottom and top layers of the studied part. We consider here that both the top and bottom surface of the part are accessible. In the case where the bottom surface of the tested sample is not accessible, the simulations must be performed in reflection mode. In this configuration, the heat source must be moved, so that the camera has a view of the surface under test during excitation. This will affect the spatial distribution of the heating power density.

For the tests, three configurations will be used, shown in Fig.1.

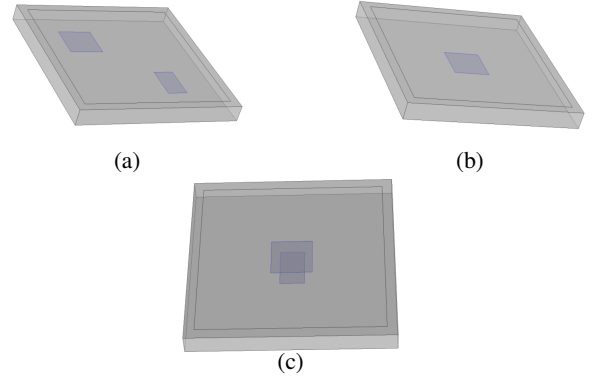


Fig. 1: Sketches of the different configurations: a) Configuration n°1, b) Configuration n°2, c) Configuration n°3

1) *Case 1: homogeneous bi-material part:* The part consists of two layers, each with a thickness of 2.5 mm . The first layer is composed of aluminum, while the second layer is composed of steel, with the parameters listed in Tab.I and Tab.III. The evolution of the temperatures within the lower and upper layers for the n°1 configuration is illustrated in Fig.2 and in Fig.3 for the n°2 configuration.

It is noticed that in the case of the configuration n^{irc}1, the evolution of the temperature given by our method is

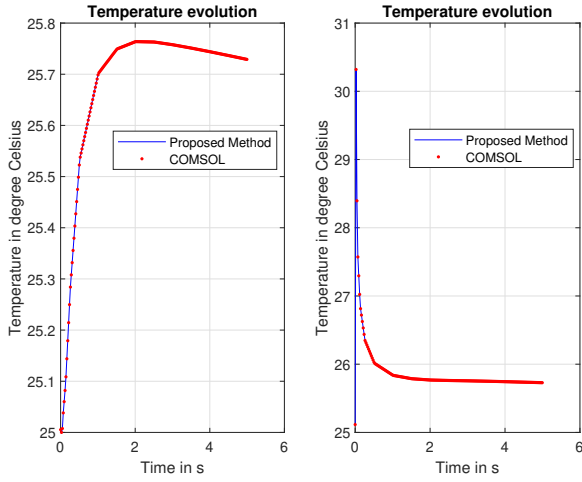


Fig. 2: Comparison plots of the temperatures' evolution at the central point of the top and bottom layers for configuration n°1

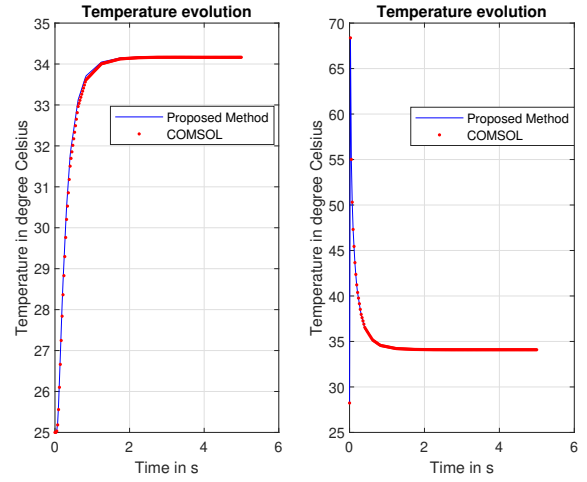


Fig. 4: Comparison plots of the temperatures' evolution at the central point of the top and bottom layers for configuration n°2

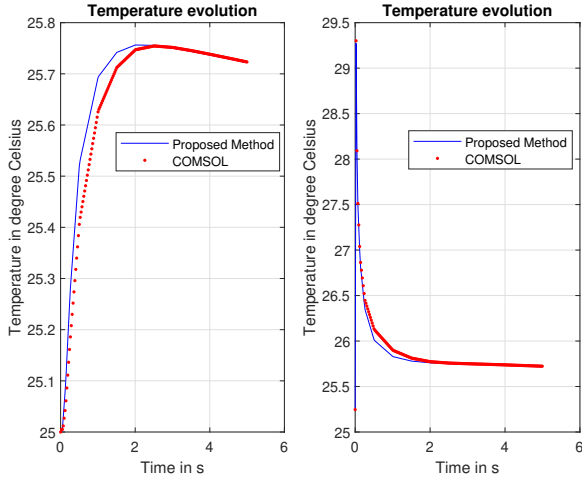


Fig. 3: Comparison plots of the temperatures' evolution at the central point of the top and bottom layers for configuration n°2

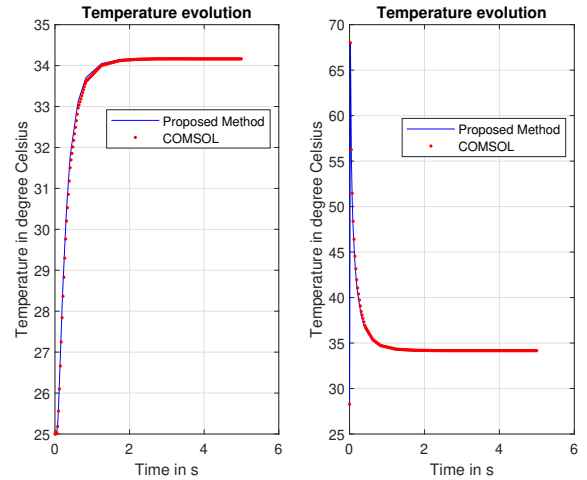


Fig. 5: Comparison plots of the temperatures' evolution at the central point of the top and bottom layers for configuration n°3

very close (mean square error $MSE = 0.01$). In the case of the $n^{irc}2$ configuration, the similarity of the curves is less ($MSE = 0.14$). This is related to the fact that in the second configuration the defect is located in the center of the part, below the point at which the measurement of the temperature evolution is taken, coupled with the fact that the delamination is located at the interface between two different materials, thus having particularly different thermal conductivities.

2) *Case 2: inhomogeneous CFRP part:* The part consists of four layers, each with a thickness of 0.2 mm with the parameters listed in the tables Tab.I, Tab.II and Tab.III. The evolution of the temperatures within the lower and upper layers for the $n^{\circ}2$ configuration is illustrated in Fig.4 and in Fig.5 for the $n^{\circ}3$ configuration.

The observations made for the bi-material part for the second configuration are not applicable to the part composed of CFRP. Indeed, the similarity of the curves ($MSE = 0.01$) for both the $n^{\circ}2$ and $n^{\circ}3$ configurations. These results confirm that the problems encountered in the previous case were related to the difference in thermal conductivity between the two materials.

E. Comsol: other tests

1) *Case 3: inhomogeneous CFRP part with a central defect at different depths:* The part consists of four layers, each with a thickness of 0.2 mm with the parameters listed in Tab.I, Tab.II and Tab.III. The evolution of the temperatures within the

lower and upper layers for the $n^{\circ}2$ configuration as a function of the depth of the central defect is illustrated in Fig.6.

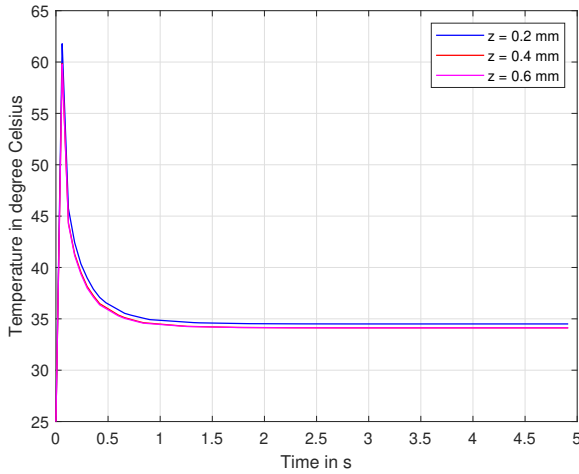


Fig. 6: Temperature evolution of the top surface depending of the depth of the central defect

The deeper the delamination, the lower the equilibrium temperature reached at the end of the observation. This can be explained by the fact that, the closer a defect is to the surface, the greater the reflected heat flux will be, which will cause a greater increase in the surface temperature of the part. The differences between these curves are minimal, for example between the one obtained for a defect at $z = 0.2 \text{ mm}$ and the one for a defect at $z = 0.6 \text{ mm}$, the mean square error $MSE = 0.06$. From this observation it is possible to note that, in an inverse problem approach, the determination of the exact depth of a defect within a part will require a very particular precision.

2) *Case 4: two inhomogeneous CFRP parts, one oriented and the other uniaxial with a central defect:* The part consists of four layers, each with a thickness of 0.2 mm with the parameters listed in Tab.I, Tab.II and Tab.III. The evolution of the temperatures within the lower and upper layers for the $n^{\circ}2$ configuration as a function of the orientation of the studied part (orientation defined in Tab.V and otherwise unidirectional) is illustrated in Fig.7.

The difference in the temperature evolution in the upper layer between an oriented part and a unidirectional part is moderate, with a $MSE = 0.26$. The difference is indeed significant, linked to the difference between a unidirectional material, thus quasi-isotropic, and an anisotropic material.

3) *Case 5: inhomogeneous CFRP part, with and without central defect:* The part consists of four layers, each with a thickness of 0.2 mm with the parameters listed in the tables Tab.I, Tab.II and Tab.III. The evolution of the temperatures within the lower and upper layers for the $n^{\circ}2$ configuration as a function of the presence (or not) of the central defect is illustrated in Fig.8.

The presence of a defect in a part will have a moderate impact on the temperature evolution curves in the upper and

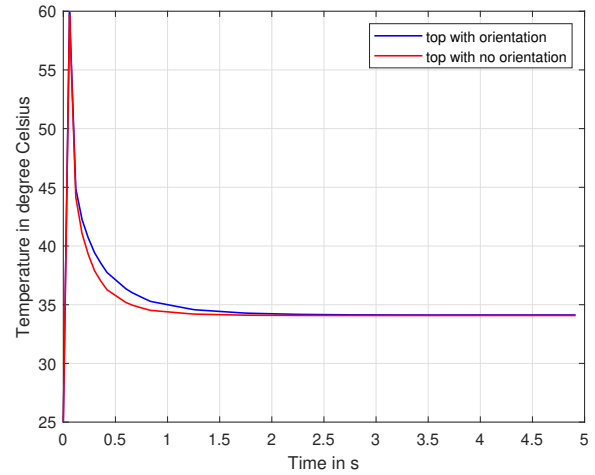


Fig. 7: Temperature evolution of the top surface for an unilateral piece and an oriented piece

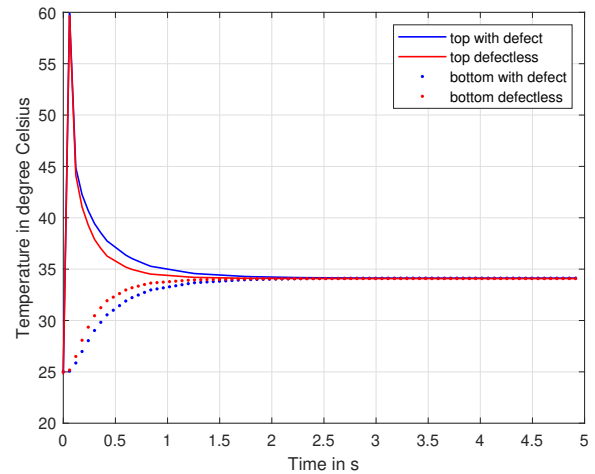


Fig. 8: Temperature evolution of the top surface depending on the presence of a defect

lower layers. Indeed, in the case where a defect is present, a slight increase in temperature is observed after the reflection of the chalking flux on the defect, and in parallel a decrease in temperature in the lower layer. The MSE between these curves (average lower and upper layer) is $MSE = 0.18$, slightly lower than when comparing an oriented part with a unidirectional part. It is important to specify that the defect is in this case very thin, with a thickness of 10^{-3} mm . This parameter has an influence, which will be studied in case $n^{\circ}6$. The figure Fig.8 allows us to observe that with the presence (or not) of defect, the equilibrium temperature remains the same.

4) *Case $n^{\circ}6$: inhomogeneous CFRP part, with central defect with different thicknesses:* The part consists of four layers, each with a thickness of 0.2 mm with the parameters listed in Tab.I, Tab.II and Tab.III. The evolution of the temperatures within the lower and upper layers for the $n^{\circ}2$ configuration as

a function of the thickness of the central defect is illustrated in Fig.9.

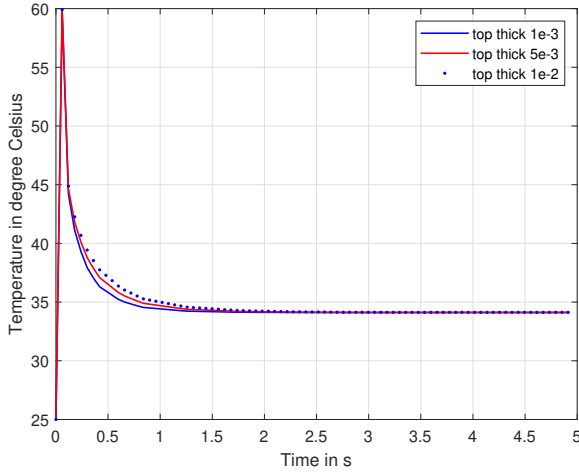


Fig. 9: Temperature evolution of the top surface depending of the thickness of the central defect at $z = 0.4 \text{ mm}$

It is observed that the temperature evolution is impacted by the thickness of the defect. Indeed, the thicker the defect observed, the greater the heat increase observed in the upper layer. This knowledge, merged with those obtained by the study of the other cases presented in this article, allow us to have a priori information, useful for an inverse problem solving approach of determination and characterization of defects within an inhomogeneous part by thermographic inspection.

It is necessary to note that the numerically calculated temperatures have a high accuracy. In order to simulate the raw thermograms obtained experimentally, the temperature values have to be rounded up to one or two decimal places. In this way, a minimum temperature resolution is assumed and the sensitivity of an infrared camera is simulated. Once the temperature values resulting from the calculations are rounded according to the assumed sensitivity, they can be processed by the proposed techniques. Indeed, if the sensitivity of an infrared camera is not simulated assuming a minimum temperature resolution, the final results are more favorable but less realistic.

F. Computational costs

The main interest of this convolution approach was to propose an alternative with lower computational costs. In order to provide an objective comparison with the performance of the Comsol Multiphysics FEM approach, the same observation period of the heat transfer evolution and the same time step were used. In order to obtain a reliable representation of the computational costs, each approach was run with different heat transfer configurations in inhomogeneous media. It is noted that the Comsol Multiphysics simulations were run with a normal mesh. The resulting average computational cost results on a computer with an Intel Core i7 10875H CPU (2.30 GHz) are available in Table Tab.VII.

Computational costs [s]	
Convolution approach	2.36
Comsol Multiphysics approach	139.44

TABLE VII: Carbon-Fiber Reinforced Polymer Heat transfer, Computational costs

From the point of view of the computational costs involved, the convolution approach is, as expected, much lighter than the FEM approach. Such a decrease in computational costs while using a CPU implementation opens doors for the fast generation of heat transfer datasets.

V. CONCLUSION

A convolution approach to heat transfer in an anisotropic material has been described in this paper. The results obtained and their quasi-coincidence with the results obtained by Comsol Multiphysics have been demonstrated for two different configurations. Tests were then carried out to determine the influence of the different parameters inherent to the implementation of the heat transfer problem in a fibered polymeric part. The impact of these parameters could be quantified, allowing to gather a priori information that can be used to define an inverse problem solving for the determination and characterization of defects in a CFRP.

At the same time, the computational efficiency of our convolution approach has been highlighted, underlining the possibility of developing dynamic heat transfer data sets in CFRPs in a low-cost manner. Such datasets can be exploited to determine the presence of defects in a CFRP and its parameters, for example through a neural network approach [14]. In future work, improvements in the management and duration of lighting, which is defined here as uniform, can be considered, as well as the development of solutions to the underlying inverse problem.

VI. ACKNOWLEDGEMENTS

REFERENCES

- [1] P. Wen, Y. Hon, M. Li, and T. Korakianitis, "Finite integration method for partial differential equations," *Applied Mathematical Modelling*, vol. 37, no. 24, pp. 10092–10106, 2013.
- [2] A. Ratsakou, C. Reboud, A. Skarlatos, and D. Lesselier, "Fast simulation approach dedicated to infrared thermographic inspection of delaminated planar pieces," in *AIP Conference Proceedings*, vol. 2102, p. 120004, AIP Publishing LLC, 2019.
- [3] Q. Fang and X. Maldague, "A method of defect depth estimation for simulated infrared thermography data with deep learning," *Applied Sciences*, vol. 10, no. 19, p. 6819, 2020.
- [4] H. Carslaw and J. Jaeger, "Conduction of heat in solids," *Oxford Press*, 1959.
- [5] J. Macias, J. Bante-Guerra, F. Cervantes-Alvarez, G. Rodríguez-Gattorno, O. Arés-Muzio, H. Romero-Paredes, C. Arancibia-Bulnes, V. Ramos-Sánchez, H. Villafán-Vidales, J. Ordóñez-Miranda, *et al.*, "Thermal characterization of carbon fiber-reinforced carbon composites," *Applied Composite Materials*, vol. 26, no. 1, pp. 321–337, 2019.
- [6] S. Bard, F. Schönl, M. Demleitner, and V. Altstädt, "Influence of fiber volume content on thermal conductivity in transverse and fiber direction of carbon fiber-reinforced epoxy laminates," *Materials*, vol. 12, no. 7, p. 1084, 2019.
- [7] V. Mityushev, Y. Obnosov, E. Pesetskaya, and S. Rogosin, "Analytical methods for heat conduction in composites," *Mathematical Modelling and Analysis*, vol. 13, no. 1, pp. 67–78, 2008.

- [8] C. Li and D. Lesselier, "On homogenization of fiber-reinforced polymers," *Journal of applied physics*, 2021.
- [9] V. Vavilov and S. Pawar, "A novel approach for one-sided thermal nondestructive testing of composites by using infrared thermography," *Polymer testing*, vol. 44, pp. 224–233, 2015.
- [10] N. Saeed, N. King, Z. Said, and M. A. Omar, "Automatic defects detection in cfrp thermograms, using convolutional neural networks and transfer learning," *Infrared Physics & Technology*, vol. 102, p. 103048, 2019.
- [11] B. Chiwu, T. Qingju, L. Junyan, and W. Yang, "Inspection on cfrp sheet with subsurface defects using pulsed thermographic technique," *Infrared Physics & Technology*, vol. 65, pp. 117–121, 2014.
- [12] R. Waugh, J. Dulieu-Barton, and S. Quinn, "Modelling and evaluation of pulsed and pulse phase thermography through application of composite and metallic case studies," *Ndt & E International*, vol. 66, pp. 52–66, 2014.
- [13] N. Moës, E. Béchet, and M. Tourbier, "Imposing dirichlet boundary conditions in the extended finite element method," *International Journal for Numerical Methods in Engineering*, vol. 67, no. 12, pp. 1641–1669, 2006.
- [14] Y. Duan, S. Liu, C. Hu, J. Hu, H. Zhang, Y. Yan, N. Tao, C. Zhang, X. Maldague, Q. Fang, *et al.*, "Automated defect classification in infrared thermography based on a neural network," *NDT & E International*, vol. 107, p. 102147, 2019.